# Developing a passive house with a double-skin envelope based on energy and airflow performance

Article (Accepted Version)

# Developing a Passive House with a Double-Skin Envelope Based on Energy and Airflow Performance


## Abstract

This research originated from an interest in developing products with a holistic and interdisciplinary systems engineering approach, toward fostering sustainability. A comprehensive method which helps designers make better decisions in the earliest design stage was applied for conceptual model development and comparison. The study developed a new-design passive house with a double-skin envelope that delivers better energy consumption performance for heating and cooling relative to a conventional reference house, while achieving comfort-level indoor temperatures. A single-façade reference house was designed with the identical geometry, material and conditions of the new house living quarters, in order to demonstrate the new house performance using a valid comparison. The new house and reference house were simulated cases and were not calibrated by actual models. The energy simulations demonstrated that the heating and cooling demands of the new house were 19.1% and 18.8% lower than those of the reference house, respectively. Furthermore, fluid dynamics behavior of the air inside the double-skin envelope was analyzed to demonstrate the airflow's contribution to the energy performance. Computational fluid dynamics simulations revealed that turbulent airflow in the underground space on summer day increased heat transfer, and laminar airflow in the double-skin roof on winter night decreased such transfer.



**Keywords:** Computational modeling; Energy efficiency, Energy systems, Fluid dynamics, Numerical simulation, Partial double-skin façade.

## Abbreviations

| | |
|---|---|
| ANSI | American National Standards Institute |
| ASHRAE | American Society of Heating, Refrigerating, and Air-Conditioning Engineers |
| CFD | Computational fluid dynamics |
| DSE | Double-skin envelope |
| DSF | Double-skin façade |
| DSR | Double-skin roof |
| ES | Energy simulation |
| IPHA | International Passive House Association |
| MoWiTT | Mobile Window Thermal Test |
| PH | Passive house |
| PHI | Passive House Institute |
| RANS | Reynolds-averaged Navier-Stokes |
| RNG | Re-Normalization Group |
| TARP | Thermal Analysis Research Program |

## 1. Introduction

Passive house (PH) design has been a building sector solution to improve the quality of human life while supporting ecosystems since its introduction in 1991 (International Passive House Association (IPHA) 2010a). The Passive House Institute (PHI) defines a PH as a building for which thermal comfort (ISO 7730) can be achieved solely by post-heating or post-cooling of the fresh air mass, which is required to achieve adequate indoor air quality conditions without the need for additional recirculation of air (IPHA 2010b).

Since early 1980s, PHs, double-skin façades (DSF) and double-skin roofs (DSR) have begun to play an important role in environmentally friendly and energy-efficient building design. In 1979, Hartweg (1984) developed a zero-energy design house with DSR, underground space, and pipes. The DSF and DSR of this house acted as a thermal buffer, reducing heating and cooling demands. The design included a water pool as the thermal mass to store solar energy. Additionally, underground space and pipes of the house benefited from earth ambient temperature year round. However, the house had three major drawbacks.

1) Design required mechanical ventilation for the underground pipes.

2) Design required long underground pipes to be laid with a slope.

3) Double-skin cavity built up humidity, caused by the water pool.

In the early 1990s, double-skin designs gained momentum when architects began to have greater interest in energy-efficient buildings as the demand for such buildings grew. However, the external appearance was limited to an inner conventional façade with an additional façade made of glass panes and metal frame on the building outside (Hilmarsson 2008). By using the cavity as a natural or mechanical ventilation system, the energy needed for ventilation was reduced. Since the early 1990s, studies and applications have lacked a surrounding thermal zone from top to bottom, which improves the heat transfer rate around the house and an underground space to utilize earth ambient temperature.

Recently, it has been shown that DSF is effective in energy conservation (Xu and Ojima 2007; Chan et al. 2009; Shameria et al. 2011; Aksamija 2009; Çetiner and Özkan 2005; Yılmaz and Çetintaş 2005). Among the wind-driven ventilation techniques forwarded by Khan et al. (2008), DSR for building roofs was considered an effective method for energy-saving designs. As for underground space and pipes, Rabah (2005) and Zhu et al. (2010) referred to effective

underground warming and cooling by ducts and tunnels utilizing ground heat. Underground space heating based on the energy-storage capacity of the soil improves the indoor environment by pre-heating outside air in winter. In summer, an underground space's vent connected to an earth tube was open to suck fresh air from outside and cool it in the underground space.

Literature review of DSF, DSR and underground space showed that although there were academic studies on DSF and DSR separately, there has been no study of their full or partial integration.

Based on these findings, the study aimed to develop a new-design PH with full surrounding thermal zone, which would deliver superior performance in energy consumption for heating and cooling while achieving comfort-level indoor temperatures relative to a conventional reference house. Hereafter, any integrated system of DSF and DSR including underground space and earth tube (if existent) shall be referred to as double-skin envelope (DSE).

## 2. Methods

A comprehensive method which included conceptual new house and reference house development, energy performance comparison of new house with reference house based on energy simulation, and airflow performance analysis of new house based on energy and computational fluid dynamics (CFD) simulation coupling without iteration, was applied for achieving the goal of this study.

### *2.1. Developing a New Design Passive House*

A new house with the first partial double-skin façade (DSF) design integrated with a double-skin roof (DSR), underground space and earth tube, was introduced by eliminating the shortcomings of the existing double-skin house designs. Main parameters of the building

envelope affecting energy performance are building geometry, its orientation and location (Sadineni et al. 2011; Tavares and Martins 2007; Yıldız and Arsan 2011; Wang et al. 2009; Tommerup et al. 2007; Filippin et al. 2005; Wang et al. 2009; Persson et al. 2006; Hassouneh et al. 2010; Lee et al. 2006; Liu et al. 2010). Main design criteria for the new house are energy performance (building geometry, orientation and location/climate), architectural design (ergonomics, maintenance and aesthetics), cost effectiveness (materials and simplicity) and Passive House Institute standard. The new house geometry is designed by integrating partial DSF, DSR, underground space and earth tube into a naturally ventilated, single-story PH (Appendix). The new house is aligned on an east-west axis in Istanbul, where strong incident solar radiation may be captured. Istanbul's (latitude N 40° 58' and longitude E 28° 49'), climate is characterized as a warm, marine and subtropical. Summer weather in Istanbul is warm, where a maximum daily average dry-bulb temperature is 24.2 °C in August. Winters are cold and wet, where a minimum daily average dry-bulb temperature is 4.9 °C in February. Spring and autumn are mild, but often wet and unpredictable. Istanbul has persistently medium to high humidity. In the present study, energy modeling and simulations on different combinations of the system components, and sensitivity analysis were used to support the design process of the new house. The DSE design adds a second envelope on the roof, partly onto the floor, the north and south walls. Inclination of the DSR, underground space and earth tube shapes, and north-side and south-side partial DSF sizes, contribute to thermal energy performance of the house. Figure 1 shows the basic design components of the new PH: 1) Underground space; 2) Living quarters; 3) DSR; 4) South-side partial DSF; 5) North-side partial DSF; 6) Earth tube; 7) Inlet air vent; 8) Outlet air vent; 9) North-side partial DSF bottom opening; 10) South-side partial DSF bottom opening; 11) DSR north opening; 12) DSR south opening; 13) Earth tube opening; 14) Glazing.

The new PH is designed to operate with an underground space inlet and roof outlet vents that are open in summer and closed in winter. Vents of the new house control the airflow and thereby temperatures in the DSE. Major features considered in the new house design to save auxiliary energy within the indoor human comfort range are as follows:

1) Full thermal zone from top to bottom, with a DSR and partial DSF walls to improve the heat transfer rate around the house (Figure 2);

2) Underground space to utilize earth ambient temperature;

3) Simplified earth tube with air vents for ventilation in summer;

4) Radiant Barrier Systems (RBS) to avoid overheating in summer;

5) Envelope (excluding underground space and earth tube) built with structural insulated panels made up of Styropor for low conductivity and easy assembly;

6) Compact envelope design with minimized area in contact with outdoor air;

7) Double-glazed southern windows to maximize solar gain in winter, to benefit from natural daylight;

8) Minimized northern double-glazed area to prevent overcooling in winter;

9) Eliminated western and eastern glass to prevent overheating in summer;

10) Single-pane window on exterior partial southern DSF wall to increase solar radiation gain on winter days;

11) Well-insulated and unleaded PVC frames with low conductivity for both single-pane and double-pane windows;

12) Thermal insulation including foundation to retain earth ambient heat in winter;

13) Natural ventilation to provide a less expensive and simple way for cooling in temperate regions where nocturnal air temperature is lower than the comfort temperature, and dissipate heat accumulated during the day;

14) Shades to provide shading in summer.

*2.2. Conceptual Reference House Development*

To demonstrate that the new house has better performance, a reference house was designed with naturally ventilated single façade living quarters (Figure 3).

The size, design and material of the reference house living quarters are identical with those of the new house for valid performance comparison.

*2.3. Energy Performance Comparison of New House with Reference House Based on Energy Simulation*

In parallel with Azarbayjani (2010), the simulated new house was compared with the simulated reference house. The performance comparison was based on energy simulations of the new and reference houses.

Energy simulation (ES) program, EnergyPlus 8.0, was used to model the buoyant flow of air between the inner and outer panes of the DSE and to simulate heat transfer in the cavity based on a nodal approach. The main objective of the ES was to generate performance data, i.e., heating and cooling demand and indoor temperature for both the new and reference houses, by estimating thermal and airflow profiles inside the DSE during extreme summer and winter conditions. Additionally, ES provided building envelope average surface temperature and average airflow rate at vents and openings, to serve as boundary conditions in a CFD model for analyzing the fluid dynamics behavior of air inside the DSE.

*2.3.1. Energy Model Setup*

The new house with six thermal zones and reference house with one thermal zone were established with EnergyPlus 8.0 for ES. For solid materials, all thermo-physical dependencies,

corner and thermal bridge effects are ignored. Instead, conductivity, density and heat capacity at each time step are considered. Solar distribution was set as full exterior with reflections in "Building" class. "Surface Convection Algorithm Inside", default indoor surface heat transfer convection algorithm to be used for all zones, was set as TARP (Thermal Analysis Research Program using variable natural convection based on temperature difference by ASHRAE (American Society of Heating, Refrigerating, and Air-Conditioning Engineers) and Walton). "Surface Convection Algorithm Outside", default outside surface heat transfer convection algorithm to be used for all zones, was set as MoWiTT (Mobile Window Thermal Test using correlation from measurements by Klems and Yazdanian for smooth surfaces). Conduction Finite Difference was used as "Heat Balance Algorithm". "Timestep" used in the Heat Balance Model calculation for heat transfer and load calculations, was selected as 30 timesteps per hour. Istanbul weather data available through the US Department of Energy (2001) were used, including temperature, relative humidity, wind, and solar insolation. Wind and infiltration calculations are conducted by AirflowNetwork of ES. Temperatures and perimeters of underground space and the earth tube were defined with the C-factor and F-factor methods, as advised by American National Standards Institute (ANSI)/American Society of Heating, Refrigerating, and Air-Conditioning Engineers (ASHRAE) [2007a; 2007b]. Winter/summer vent and shade schedules were introduced to open all air vents and close the south-side partial DSF shades from 5 May through 1 October (summer period). Thermal Comfort Model AdaptiveCEN15251 is set for internal gains, contaminant rates for occupants in the living quarters. Each pair of windows on the south side of the living quarters has 1084 mm × 2384 mm outside shades, which screen the sun in summer. In order to achieve a cost-effective solution, the heating set-point was defined as 18 °C between 7:00 and 22:00, and 14 °C otherwise. Likewise, the cooling set-point was defined as 26 °C between 7:00 and 22:00, and

30 °C otherwise. Lighting and electric equipment design levels were set to 300 W and 5.38 W/$m^2$, respectively.

*2.3.2. Energy Zones of New House and Reference House*

The maximum height of the new house above ground was 4515 mm; with length 5028 mm and width 7136 mm. Maximum room height was 3976 mm. The window area comprised 29.1% of the south façade including the south-side partial DSF, and 17% excluding. Total floor area of the new house was 36 $m^2$ (2 residents × 18 $m^2$/occupant). A breakdown of energy zones and their components are presented in Figure 4 described in Table 1.

In Zone 1 (Figure 4), underground space of approximate volume 34 $m^3$ is connected to the earth tube, south and north-side partial DSFs through air vents. Underground space uses earth ambient temperature at maximum depth of 2 meters below the ground. Underground space is made of 100-mm-thick lightweight concrete, a low R factor material, to benefit from earth ambient temperature year round. Two of the air vents on the top are 700 mm × 1600 mm in size to facilitate easy maintenance. One of the air vents that connect underground space to the earth tube is 400 mm × 800 mm in size. All of the air vents in the house are constructed with 0.5-mm-thick galvanized steel on top and 88.9-mm-thick Styropor at the bottom.

In Zone 2 (Figure 4), the living quarters of the new house is wrapped with five thermal zones: underground space connected to the earth tube, south and north-side partial DSFs that are connected to the DSR. The living quarters has a rectangular shape with an open plan, but its interior design is not within the scope of the study. Its 1:2.2 ratio of interior floor area (approximately 36 $m^2$) to exterior surface area (~ 80 $m^2$) shows the energy efficiency of the geometry. Styropor 88.9-mm-thick is used for the floor, ceiling and walls of the living quarters. The living quarters has two (1600 mm × 1600 mm) double-pane (with 6.3 mm air gap) low-e

glazing on the south side for daylight and two (800 mm × 800 mm) double-pane (with 6.3 mm air gap) low-e glazing on the north side for ventilation. Also on the north side, a 2384 mm × 800 mm size door made of a metal sheet with 25-mm-thick insulation was modeled for the living quarters. The two (1084 mm × 2384 mm) outside shades with RBS above the south windows are also included.

In Zone 3 (Figure 4), unlike normal ventilated attics with an only connection to outside, the DSR is connected to south and north-side partial DSFs through two (150 mm × 2000 mm) air openings. North inclination of the DSR reduces not only the solar irradiation for summer but also the air volume at north side of Zone 2, the living quarters, for winter. The experiments of Irwan et al. (2009) identified the optimum roof pitch angle for thermal and energy saving potential in a local climate. The DSR slope angle was selected as 15°, within the 10°–20° range of the latter study. Combination of a high-gloss roof and low-gloss ceiling finish underneath is generally used in the industry. Chang et al. (2008) designed prototypical double roofs inspired by the concepts of both the double-skin structure and RBS, specifically to reduce solar heat gain from the roof. Ong (2011) tested six laboratory-sized passive roof designs side-by-side consecutively over a number of days, finding that a bare metal roof with insulation underneath resulted in the highest roof temperature. Based on these studies, the top skin of the DSR was composed of a 0.5-mm-thick white painted galvanized steel sheet for effective passive solar design on top and 88.9-mm-thick Styropor, with a RBS at the bottom. Lai et al. (2008) used inclined parallel plates with an upper plate heated by a lighting system to simulate DSRs exposed to solar radiation. Heat transfer experiments were carried out for different inter-plate spacing and inclined angles. Lai et al. also showed that placing a low-cost radiant barrier on top of the lower plate structure could be very effective in preventing roof heat from entering

the building. Susanti et al. (2008) targeted a reduction of roof solar heat gain through the use of natural ventilation in a roof cavity. Natural ventilation in that cavity appeared to be highly applicable to solar incidence discharges. In parallel with these studies, the air gap in the DSR was set to 150 mm. The sides of the DSR were closed by 88.9-mm-thick Styropor with adequate conductive insulation.

In Zone 4 (Figure 4), the south-side partial DSF uses 88.9-mm-thick Styropor for the floor and walls. 0.5-mm-thick galvanized steel sheets on top and 88.9-mm-thick Styropor with radiant barrier at the bottom are used for the ceiling. The south-side partial DSF is connected to the underground space through a 700 mm × 1600 mm air vent, DSR through a 150 mm × 2000 mm opening, and outside through an 828 mm × 1800 mm air vent. Window shades with radiant barriers, inside the cavity of the south-side partial DSF are directly behind 6-mm single-pane (2400 mm × 1600 mm) glazing.

In Zone 5 (Figure 4), the north-side partial DSF is connected to the underground space through air vents. Styropor 88.9-mm-thick is used for the floor and walls of this DSF. 0.5-mm-thick galvanized steel sheets on top and 88.9-mm-thick Styropor with radiant barrier at the bottom are used for the ceiling. The north-side partial DSF is connected to the underground space through a 700 mm × 1600 mm air vent and DSR through a 150 mm × 2000 mm opening.

In Zone 6 (Figure 4), the earth tube, which has an approximate volume of 1.6 $m^3$, is made of 100-mm-thick lightweight concrete. Through a 700 mm × 800 mm air opening at the back, outside air enters the tube and passes to the underground space through a 400 mm × 800 mm air vent in summer. Height of the earth tube is 2000 mm, the same as that of the underground space.

Living quarters' of the new and reference houses have identical geometry and installations for valid comparison. Maximum height of the reference house above ground is 4224 mm.

In Zone 1, the living quarters of the reference house is not wrapped by any thermal zone, and incorporate a single-skin roof, RBS, windows and shadings. The single-skin roof is designed with the same Styropor thickness (88.9 mm) as the living quarters of the new house. Material properties of the living quarters and their components are the same as that of the new house.

*2.4. Airflow Performance Analysis of New House Based on Energy and CFD Simulation Coupling without Iteration*

Fluid Dynamics behavior of the air inside DSF, DSR and underground space was analyzed in order to demonstrate airflow's contribution to the energy performance. Airflow performance analysis of the new house was based on energy and computational fluid dynamics simulation coupling without iteration.

Azarbayjani (2010) suggested that coupling CFD simulation with an ES gives more accurate results than a CFD simulation or ES alone in building energy analysis. Zhai and Chen (2005) coupled ES and CFD simulation with different coupling methods, and validated the coupled simulations using four sets of experimental data from the literature. Comparison of the simulated results with the experimental/empirical data revealed advantages of the coupled building simulation over the separate ES and CFD simulations. Zhai et al. (2002) described efficient approaches to integrate ES and CFD, such as static and dynamic coupling strategies, in order to bridge discontinuities of time scale, spatial resolution and computing speed between ES and CFD programs. In principle, a fully iterated ES and CFD coupling program can provide a solution that is equivalent to the conjugate heat transfer method, provided that the ES program

generates grids with sufficiently high resolution to model any significant temperature variations.

The CFD simulation program, Fluent 14.0 was used in the present study to solve turbulent airflow inside the DSF in extreme summer and winter conditions. In parallel with Azarbayjani (2010), Zhai and Chen (2005) and Zhai et al. (2002), a manual static coupling process with one-step data feed from energy to CFD simulation was executed. Air inside the DSE was the only domain under investigation, and it was separated into the following subzones: 1) Underground space; 2) DSR; 3) South-Side partial DSF; 4) North-Side partial DSF (Figure 4).

*2.4.1. Boundary Conditions*

Results of EnergyPlus were entered as boundary conditions into Fluent. During summer day time with open inlet and outlet vents, the underground space vent was defined as the mass flow inlet and the roof vent as the pressure outlet of the air domain. Backflow can occur, depending on local density and temperature properties. For natural convection, static pressure at the openings was set as gauge pressure in Fluent. Gravity was taken into account, and zero pressure difference between the inlet and outlet was calculated. An operating pressure equal to atmospheric pressure was assumed, owing to the fact that pressure variations around the static pressure are small. The external and internal walls were established as wall boundaries of the air domain. The external and internal walls were defined as adjacent to the external environment and living quarters, respectively.

For winter night time with closed inlet and outlet vents, fluid boundary conditions were modeled as a closed circuit because there was neither inlet nor outlet. In other words, the inlet and outlet were considered wall boundaries and the DSE domain was sealed with no air exchange outside the domain.

For both the external and internal wall boundaries of air inside the DSE, the corresponding EnergyPlus output on surface temperatures (°C) is illustrated in Figure 5. Additionally, the side walls of the air vents and openings covered with Styropor were assumed to be adiabatic.

Air density was calculated based on the Boussinesq approximation. The Boussinesq approach for buoyancy-driven flows assumes that the density is constant in all equations, except for the buoyancy term in the momentum equation:

$$(\rho - \rho_0)g \approx -\rho_0 (T - T_0), \quad (1)$$

where $\rho$ is actual density, $\rho_0$ is the constant density of the flow, T is actual temperature, and $T_0$ is the operating temperature. Based on the Boussinesq approximation that is valid when $\Delta T = (T - T_0) \ll 1$, the actual density is

$$\rho = \rho_0 (1-\beta \Delta T), \quad (2)$$

where $\beta$ is the thermal expansion coefficient.

There was only one calculation domain and the properties of this fluid domain are defined in Table 2.

The infiltration of the DSR, south-side partial DSF and north-side partial DSF calculated in EnergyPlus was taken into account only for summer in Fluent. In summer, the DSR, north-side partial DSF and south-side partial DSF surfaces all behaved as outlets, with 0.0043, 0.0036 and 0.0049 kg/s mass flow rates, respectively. This infiltration was added to the outlet target mass flow rate (kg/s) in the Fluent boundary conditions.

*2.4.2. Model Grid*

The airflow model of the new house DSE was determined by the Rayleigh number (*Ra*). This number characterizes natural convection flows, which can be laminar ($Ra < 6\times10^4$), transitional

($6\times10^4 < Ra < 10^9$), or turbulent ($10^9 < Ra$). For an appropriate selection of airflow model, Rayleigh numbers for the following zones should be calculated for summer day time and winter night time extremes: 1) Underground space; 3) DSR; 4) South-side partial DSF; 5) north-side partial DSF (Figure 4).

Wall distances of the new house DSE were estimated by the Reynolds number (*Re*). *Re* is calculated based on EnergyPlus output for average airflow rates at vents and openings ($m^3/s$) and incompressibility of the airflow. For summer day time extreme, EnergyPlus output for average airflow rates and temperatures at the following six nodes, and average surface temperatures including the glazing was produced (Figure 6): 1) Underground space inlet vent; 2) Roof outlet vent; 3) South-side partial DSF bottom opening; 4) North-side partial DSF bottom opening; 5) DSR north opening; 6) DSR south opening.

For winter night time extreme, output for average airflow rates was generated at the following four nodes (Figure 6): 3) South-side partial DSF bottom opening; 4) North-side partial DSF bottom opening; 5) DSR north opening; 6) DSR south opening. In this case, the underground space inlet vent and roof outlet vent are excluded, because they are treated as walls. Also, output of all surface temperatures is generated. Airflow rates inside the zones can be calculated provided that the flow is incompressible. Since density variation of the fluid is negligible and the flow is steady state, the Mach number (*Ma*) is calculated at 0.0002 for the maximum velocity. Because this is less than 0.3, airflow in summer and winter is assumed incompressible. Then, based on flow cross sections, vent (Table 3) and opening airflow velocities (Table 4) produced by EnergyPlus, airflow rates inside the zones in summer and winter (Table 5) were deduced. The relevant vent or opening with the maximum zone velocity was chosen. Thus, *Re* for summer and winter was calculated as seen in Table 5. The model

airflow was determined as turbulent in every zone except for the DSR based on its *Ra*, which was between $6\times10^4$ and $10^9$ for summer day time extreme. As for winter night time extreme, the model airflow was determined as turbulent in every zone except for the DSR based on its *Ra*, which was between $6\times10^4$ and $10^9$.

*Re* is basically calculated using zone hydraulic diameters, airflow rates and temperatures, yielding air density and dynamic viscosity. The area of interest is airflow in the zones rather than at vents and openings. However, model airflow was initially determined based on EnergyPlus output of node airflow rates at the vents and openings output. Then, the airflow models were further elaborated based on Fluent output of airflow characteristics in the zones. To visualize the various responses to the DSE while considering the computational resources available for this research, a 3D mesh of the DSE for both summer and winter configurations was set up according to dimensions of the fluid geometry. Accurate analysis of convective airflows requires precise calculations around boundaries. A hexahedral scheme was used, because the fluid geometry was based on square section elements. A small size mesh was generated near the walls, where laminar flows were created. The wall treatment was not applied at the vents, openings, or around the adiabatic walls of the openings. However, being the main object of interest, the wall treatment was applied to the underground space, DSR, south-side partial DSF and north-side partial DSF zones. Eventually, a single-mesh model was used for both summer and winter cases, taking the minimum estimated wall distances into consideration for the first layer. Wall distances (for y+ = 1) were estimated as 16, 4, 3 and 6 mm for the underground space, DSR, south-side partial DSF, and north-side partial DSF, respectively.

As a result, a non-uniform grid of $3.5\times10^6$ cells for the cavity, with 0.916 minimum orthogonal quality and $6.31 \times 10^{-2}$ average skewness, was produced. Grid-independence studies show that

this meshing gives results with the most reasonable accuracy per computing time.

*2.4.3. Numerical Methods*

Turbulence was modeled via the RNG k-$\varepsilon$ turbulence model. A second-order upwind spatial discretization scheme was used. A Semi-Implicit Method for Pressure-Linked Equations (SIMPLE) pressure-velocity coupling scheme was selected for coupling with the default options. Convergence criteria were set to $10^{-3}$ for the momentum equations and $10^{-6}$ for energy.

*2.4.4. Validation of Energy and CFD Simulation Coupling without Iteration*

In this study, test cavity of Saelens (2002), a mechanically and naturally ventilated DSF with a roller screen sun-shading device, was modelled to validate the Energy - CFD simulation coupling method because of the available full-scale reliable experimental data on solar radiation ($W/m^2$), temperature distribution ($^oC$) and airflow rate ($m^3/s$). Two cases were used for validation, model A measured at night without incident solar radiation and shading device and model B in the morning with incident solar radiation and shading device. The cases had low wind velocities of 3.6 m/sec and 3.9 m/sec, respectively, enabling an analysis without the wind effect.

Within the limitations of the energy and airflow simulation software, comparison of the simulated and measured airflow rates with the corresponding temperature confirmed the precision of the method for a manual static coupling process with one-step data feed from Energy to CFD simulation based on Saelens' (2002) and Saelens et al.s' findings (2008), Pappas and Zhai's (2008), Zhai and Chen's (2005) and Zhai et al.'s (2002) studies. In model A, error was 0.1% and in model B, 1.5% for the temperature differences between peak cavity air and outdoor air ($^oC$). As for the inlet airflow rates ($m^3/hr$) of model A and B, errors were

15.8% and -22.9%, respectively. In Saelen's test, the measurement errors were estimated about 4% for temperature and 10% for airflow rate.

## 3. Results

### *3.1. EnergyPlus Simulation Results*

EnergyPlus results demonstrated that the new house was a PH and that the reference house was nearly a PH, based on the following main PH criteria (IPHA 2010b) defined by the PHI (Table 6).

EnergyPlus generated the following results for the energy and airflow behavior of the new house.

1) The partial DSF and DSR of the new PH operating at temperatures warmer than the cold winter extremes and cooler than hot summer extremes created a thermal zone around the interior shell (Table 7).

That zone used south-side solar gain and a natural convection airflow loop initiated by earth ambient temperature to heat the cold north walls of the house, equalizing the temperature differentials on the north/south and top/bottom of the house. Thus, throughout the year, the double-skin design minimized the heat transfer rate by reducing the overall temperature difference and increasing thermal resistance year round, and evacuated a large part of the heat load on the living quarters in summer.

2) Underground space temperatures were correlated with ground temperatures (Figure 7). Based on the energy storage capacity of soil, underground space improved the indoor environment by heating air in winter and cooling it in summer.

3) In summer, annual air outflow rates ($m^3/s$) at the roof and air inflow rates ($m^3/s$) at the

underground space vent nodes were equal (Figure 8), and airflow rates at the south-side partial DSF bottom opening node were higher than in winter (Figure 9).

4) During summer day time, roof and underground space vents were open and the shading was active. Underground space vent drew fresh air from outside, and then cooled it in the underground space. As the air temperature rose in the DSFs and DSR, air was exhausted from the roof vent by natural convection (Figure 10).

Air circulation created a thermal zone colder than outside temperatures, and hence contributed to thermal performance of the house. On a summer day, air flowed from outside to the underground space (Figure 8), from the underground space to the south-side partial DSF (Figure 9), from that space to the north-side partial DSF bottom opening (Figure 11), from the DSR south opening node to the south-side partial DSF (Figure 12), and from the north-side partial DSF to the DSR north opening node (Figure 13). The highest outside temperature of 31.2 ºC, occurred on the 4$^{th}$ of July at 15:00 o'clock, was considered in the energy analysis.

5) During winter night time, roof and underground space vents were closed and the shading was inactive. As the air in underground space warmed, it rose in the DSFs and, as it got colder at the top, it fell back to the underground space by natural convection (Figure 10). Air circulation created a thermal zone warmer than outside temperatures, and hence contributed to thermal performance of the house. On winter nights, the air flowed in both directions at all nodes (Figure 8) (Figure 9) (Figure 11) (Figure 12) (Figure 13). The lowest outside temperature of -7.8 ºC, occurred on the 20$^{th}$ of February at 6:00 o'clock, was considered in the energy analysis.

*3.2. Fluent Simulation Results*

Figures generated by Fluent, depicted zone temperatures, airflow rates, static pressures and turbulent $R_e$ for summer day and winter night extremes. The airflow was predominantly symmetric. Therefore, Fluent result demonstrations were mainly given at the midsection (x-y plane) of the new house.

1) Contours of static temperatures for summer day and winter night were generated for that midsection (Figure 14). Temperatures ranged from 294–307 K for summer day and 268–281 K for winter night.

2) For summer day and winter night, vectors of velocity magnitude were produced at the aforesaid midsection (x-y plane) (Figure 15), along a streamline at the midsection of the underground space (x-z plane), inlet (x-z plane), DSR (x-y-z plane), south-side partial DSF (y-z plane) and north-side partial DSF (y-z plane) (Figure 16). Airflow rates were 0–1 m/s for summer day and 0–0.6 m/s for winter night.

3) Contours of static pressure for summer day and winter night were generated at the midsection (x-y plane) of the new house (Figure 17). The pressures were 0.1–2.9 pa for summer day and −0.7 pa to 0.3 pa for winter night.

4) Contours of turbulent *Re* (*Re_y*) for summer day and winter night were produced at the midsection (x-y plane) of the new house (Figure 18). *Re* was 0 –6771 for summer day and 0–3118 for winter night.

5) The temperature stratification for summer day and winter night, with 304 K and 265 K outdoor temperatures, respectively, showed earth ambient temperature and thermal zone contributions to energy performance of the new house (Figure 14). On summer day, underground space airflow rates maximized, especially in the vicinity of its vent, and vortices

that are major components of turbulent flow were observed in the underground space. Flow at the center of that space was determined to be turbulent, based on *Re* values that were > 4000. On summer day and winter night, pressure decreased in the y direction and heat was gradually accumulated at the DSE upper level. Airflow rates increased at the top of the north-side partial DSF and south-side partial DSF, maximizing at the DSR north and south openings. Throughout the DSR, the flow was determined to be laminar, based on *Re* values < 2300.

## 4. Discussion

### *4.1. Design Implications*

From a DSF design perspective, the study introduced two major points.

1) The first partial DSF, DSR, underground space and earth tube integration into PH architecture formed a surrounding thermal zone from top to bottom and hence, minimized energy consumption while providing required comfort.

2) The partial DSF design was more suitable for retrofitting relative to a full DSF design, because it used less building material and occupied less space, making it easier to apply to existing buildings.

### *4.2. Energy Performance*

From an energy performance perspective, there were five major findings.

1) The maximum winter heating demands for the new and reference houses were approximately 478 and 591 kWh, respectively. The new house heating demand was 19.1% lower than that of the reference house.

2) The maximum summer cooling demands for the new and reference houses were approximately 1223 and 1507 kWh, respectively. The new house cooling demand was 18.8%

lower than that of the reference house.

3) The new house mean temperature in its living quarters was 0.5% higher than that of the reference house in winter and 1.9% lower in summer, indicating that energy performance of the new house did not result from deteriorated living quarter temperatures.

4) If the roof and earth tube vents of the new house were closed during summer, the cooling demand of the house would increase 4.3%, to 1278 kWh, revealing the airflow performance contribution to the new house from a different perspective.

5) The new house delivered superior heating and cooling demands (kWh) compared to those of the reference house while achieving indoor comfort level temperatures (°C), even though the reference house design was almost a PH.

*4.3. Airflow Contribution*

It was also concluded that airflow in the new house DSE contributed to energy performance in two major ways.

1) Turbulent airflow inside the DSE and especially the underground space enhanced heat transfer through wakes and momentum transfer between fluid particles, which in turn increased the friction force and convective heat transfer coefficient. Hence, heat loss occurred on summer days when it was needed. Strong convective heat transfer from the turbulent nature of the airflow in the underground space was favorable, because the zone had greater benefit from earth ambient temperature.

2) When there was no sunshine, the convectional airflow velocity was slower than the sunny day time convection airflow. At nights, smaller pressure and temperature differences in the DSE produced a weaker flow. Slow laminar airflow in the DSR produced thermal resistance

because heat transfer via the wakes was non-existent. As airflow in DSR became less turbulent, more heat was preserved on winter nights.

## 5. Conclusion

In this study, a novel design PH with a double-skin envelope was developed with superior performance in energy consumption for heating and cooling, while achieving comfort-level indoor temperatures as compared with a conventional reference house. Eliminating the shortcomings of existing double-skin house designs, the new PH introduced the first partial DSF design, which is integrated with a DSR, underground space and earth tube to form a surrounding thermal zone from top to bottom while utilizing earth ambient temperature. Finally, the fluid dynamics behavior of air inside DSE zones demonstrated the airflow's contribution to the energy performance. A limitation of the study is an actual new house to compare the numerical results with the experimental data for measuring accuracy. Additional future research can be directed towards optimizing the design criteria of the new house along with sensitivity analysis for different climates.

**Appendix** Energy zone dimensions of new house

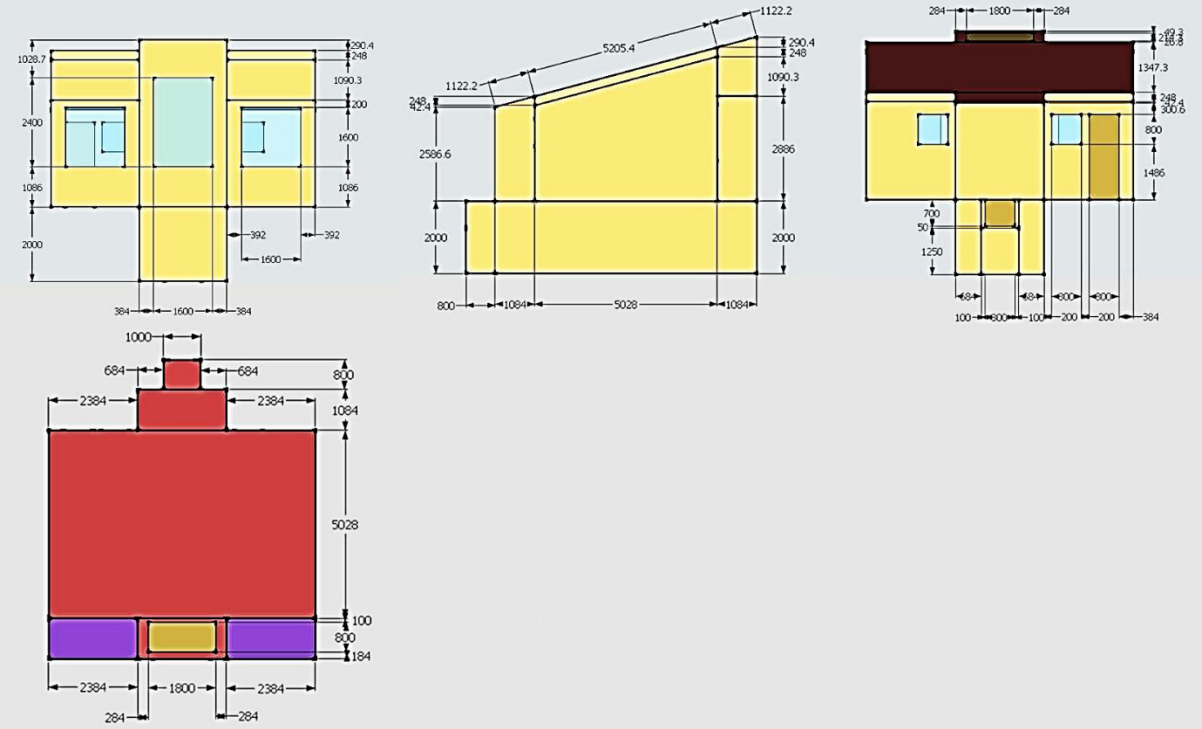


## References


[1] International Passive House Association (2010a). In: Advantages. Available at http://www.passivehouse-international.org/index.php?page_id=79 Accessed 30 Dec 2016.

[2] International Passive House Association (2010b). In: Passive House criteria. Available at http://www.passivehouse-international.org/index.php?page_id=150&level1_id=78 Accessed 30 Dec 2016.

[3] Hartweg L (1984). The Second Generation Envelope House. 5th ed. Oklahoma: Natural Energy Applied Research.

[4] Hilmarsson J (2008). Double-skin façade evaluating the viability of the component. B.Sc. Thesis, Copenhagen Technical Academy, Denmark.

[5] Xu L, Ojima T (2007). Field experiments on natural energy utilization in a residential house with a double-skin façade system. *Building and Environment*, 42(5): 2014-2023.

[6] Chan A, Chow T, Fong K, Lin Z (2009). Investigation on energy performance of double-skin façade in Hong Kong. *Energy and Buildings*, 41(11): 1135-1142.

[7] Shameri M, Alghoul M, Sopian K, Zain M, Elayeb O (2011). Perspectives of double-skin façade systems in buildings and energy saving. *Renewable and Sustainable Energy Reviews*, 15(3): 1468-1475.

[8] Aksamija A (2009). Context based design of double-skin façades. *Perkins+Will Research Journal*, 1(1): 54-69.

[9] Cetiner İ, Özkan E (2005). An approach for the evaluation of energy and cost efficiency of glass façades. *Energy and Buildings*, 37(6): 673-684.

[10] Yılmaz Z, Cetintaş F (2005). Double-skin façade's effects on heat losses of office buildings in Istanbul. *Energy and Buildings*, 37(7): 691-697.

[11] Khan N, Su Y, Riffat S (2008). A review on wind driven ventilation techniques. *Energy and Buildings*, 40(8): 1586-1604.

[12] Rabah K (2005). Development of energy-efficient passive solar building design in Nicosia Cyprus. *Renewable Energy*, 30(6): 937-956.

[13] Zhu Y, Lin B, Yuan B (2010). Low-cost green building practice in China: Library of Shandong Transportation College. *Frontiers of Energy and Power Engineering in China*, 4(1): 100-105.

[14] Sadineni S, Madala S, Boehm R (2011). Passive building energy savings: a review of building envelope components. *Renewable and Sustainable Energy Reviews*, 15(8): 3617-3631.

[15] Tavares P, Martins A (2007). Energy efficient building design using sensitivity analysis - a case study. *Energy and Buildings*, 39(1): 23-31.

[16] Yıldız Y, Arsan Z (2011). Identification of the building parameters that influence heating and cooling energy loads for apartment buildings in hot-humid climates. *Energy*, 36(7): 4287-4296.

[17] Wang N, Esramb T, Martinez L, McCulley M (2009). A marketable all-electric solar house: a report of a Solar Decathlon project. *Renewable Energy*, 34(12): 2860-2871.

[18] Tommerup H, Rose J, Svendsen S (2007). Energy-efficient houses built according to the energy performance requirements introduced in Denmark in 2006. *Energy and Buildings*, 39(10): 1123-1130.

[19] Filippin C, Larsen S, Beascochea A, Lesino G (2005). Response of conventional and energy-saving buildings to design and human dependent factors. *Solar Energy*, 78(3): 455-470.

[20] Wang L, Gwilliam J, Jones P (2009). Case study of zero energy house design in UK. *Energy and Buildings*, 41(11): 1215-1222.

[21] Persson M, Roos A, Wall M (2006). Influence of window size on the energy balance of low energy houses. *Energy and Buildings*, 38(3): 181-188.

[22] Hassouneh K, Alshboul A, Al-Salaymeh A (2010). Influence of windows on the energy balance of apartment buildings in Amman. *Energy Conversion and Management*, 51(8): 1583-1591.

[23] Lee A, Kelly H, Jagoda R, Rosenfeld A, Stubee E, Colaco J, Gadgil A, Akbari H, Norford L, Burik H (2006). Affordable, safe housing based on expanded polystyrene (EPS) foam and a cementitious coating. *Journal of Materials Science*, 41(21): 6908-6916.

[24] Liu J, Wang R, Hu R, Yang L, Liu D (2010). Energy efficiency of rural residential

buildings: a sustainable case study in Daping Village, Sichuan Province. *Frontiers of Energy and Power Engineering in China*, 4(1), 117-121.

[25] Bayraktar M (2015.) A Methodology for energy optimization of buildings considering simultaneously building envelope HVAC and renewable system parameters. Ph.D. Thesis, Politecnico di Torino, Italy - Istanbul Technical University, Turkey.

[26] Poirazis H (2004). Double-skin façades for office buildings. In: Literature Review Report EBD-R--04/3. Available at http://www.lth.se/fileadmin/energi_byggnadsdesign/images/Publikationer/Bok-EBD-R3-G5_alt_2_Harris.pdf Accessed 30 Dec 2016.

[27] Azarbayjani M (2010). Beyond arrows: energy performance of a new, naturally ventilated double-skin façade configuration for a high-rise office building in Chicago. Ph.D. Thesis, University of Illinois, USA.

[28] U.S. Department of Energy Weather Data (2001). Istanbul 170600 IWEC. Available at https://energyplus.net/weather-location/europe_wmo_region_6/TUR//TUR_Istanbul.170600_IWEC Accessed 30 Dec 2016.

[29] ANSI (American National Standards Institute)/ASHRAE (American Society of Heating, Refrigerating, and Air-Conditioning Engineers) (2007a). Standard 90.1: Energy Standard for Buildings except Low-Rise Residential Buildings - SI edn.

[30] ANSI (American National Standards Institute)/ASHRAE (American Society of Heating, Refrigerating, and Air-Conditioning Engineers) (2007b). Standard 90.2: Energy Efficient Design of Low-Rise Residential Buildings.

[31] Irwan S, Ahmed A, Ibrahim N, Zakaria N (2009). Roof angle for optimum thermal and energy performance of insulated roof. In: Proceedings of 3rd International Conference on Energy and Environment (ICEE).

[32] Chang P, Chiang C, Lai C (2008). Development and preliminary evaluation of double roof prototypes incorporating RBS (Radiant Barrier System). *Energy and Buildings,* 40(2): 140-147.

[33] Ong K (2011). Temperature reduction in attic and ceiling via insulation of several passive roof designs. *Energy Conversion and Management*, 52(6): 2405-2411.

[34] Lai C, Huang J, Chiou J (2008). Optimal spacing for double-skin roofs. *Building and Environment*, 43(10): 1749-1754.

[35] Susanti L, Homma H, Matsumoto H, Suzuki Y, Shimizu M (2008). A laboratory experiment on natural ventilation through a roof cavity for reduction of solar heat gain. *Energy and Buildings*, 40(12): 2196-2206.

[36] Zhai Z, Chen Q (2005). Performance of coupled building energy and CFD

simulations. *Energy and Buildings*, 37(4): 333-344.

[37] Zhai Z, Chen Q, Haves P, Klems J (2002). On approaches to couple energy simulation and computational fluid dynamics programs. *Building and Environment*, 37(8-9): 857-864.

[38] Saelens D (2002). Energy performance assessment of single storey multiple-skin façades. Ph.D. Thesis, Katholieke Universiteit Leuven, Belgium.

[39] Saelens D, Roels S, Hens H (2008). Strategies to improve the energy performance of multiple-skin façades. *Building and Environment*, 43 (4): 638-650.

[40] Pappas A, Zhai Z (2008). Numerical investigation on thermal performance and correlations of double-skin façade with buoyancy-driven airflow. *Energy and Buildings*, 40: 466-475.

**Table 1** Major components and materials of New House and Reference House

| **Major components and materials** | **Total Area ($m^2$)** | **Total Thickness (mm)** | **U-Values ($W/m^2K$)** | **Glass SHGC** | **Shade Control** |
|---|---|---|---|---|---|
| **New House** | | | | | |
| Zone 1 | | | | | |
| Ceiling wall - lightweight concrete | 14.7 | 101.6 | 1.098 | - | - |
| North wall - lightweight concrete | 4.5 | 101.6 | 1.098 | - | - |
| North wall - air vent Styropor | 0.3 | 88.9 | 0.406 | - | - |
| South wall - lightweight concrete | 4.7 | 101.6 | 1.098 | - | - |
| East wall - lightweight concrete | 14.4 | 101.6 | 1.098 | - | - |
| West wall - lightweight concrete | 14.4 | 101.6 | 1.098 | - | - |
| Floor wall - lightweight concrete | 17.0 | 101.6 | 1.098 | - | - |
| Zone 2 | | | | | |
| Ceiling wall - Styropor | 37.1 | 88.9 | 0.406 | - | - |
| North wall - Styropor | 15.7 | 88.9 | 0.406 | - | - |

| | | | | | |
|---|---|---|---|---|---|
| North wall - double glazings (6.3 mm air gap) | 1.3 | 18.3 | 3.058 | 0.7 | No |
| North wall - door insulation board | 1.8 | 25.4 | 1.181 | - | - |
| South wall - Styropor | 23.3 | 88.9 | 0.406 | - | - |
| South wall - double glazings (6.3 mm air gap) | 5.2 | 18.3 | 3.058 | 0.7 | Yes |
| East wall - Styropor | 16.6 | 88.9 | 0.406 | - | - |
| West wall - Styropor | 16.6 | 88.9 | 0.406 | - | - |
| Floor wall - Styropor | 11.9 | 88.9 | 0.406 | - | - |
| Floor wall - lightweight concrete | 24.0 | 101.6 | 1.098 | - | - |
| | Zone 3 | | | | |
| Ceiling wall - Styropor | 37.1 | 88.9 | 0.406 | - | - |
| North wall - Styropor | 1.5 | 88.9 | 0.406 | - | - |
| South wall - Styropor | 1.5 | 88.9 | 0.406 | - | - |
| East wall - Styropor | 1.2 | 88.9 | 0.406 | - | - |
| West wall - Styropor | 1.2 | 88.9 | 0.406 | - | - |
| | Zone 4 | | | | |
| Ceiling wall - Styropor | 1.2 | 88.9 | 0.406 | - | - |
| Ceiling wall - air vent Styropor | 0.3 | 88.9 | 0.406 | - | - |
| North wall -Styropor | 9.7 | 88.9 | 0.406 | - | - |
| South wall - Styropor | 6.9 | 88.9 | 0.406 | - | - |
| South wall - single glazing | 3.8 | 6.0 | 5.778 | 0.8 | Yes |
| East wall - Styropor | 4.7 | 88.9 | 0.406 | - | - |
| West wall - Styropor | 4.7 | 88.9 | 0.406 | - | - |
| Floor wall - Styropor | 1.4 | 88.9 | 0.406 | - | - |
| | Zone 5 | | | | |
| Ceiling wall - Styropor | 2.7 | 88.9 | 0.406 | - | - |
| North wall -Styropor | 6.1 | 88.9 | 0.406 | - | - |
| South wall - Styropor | 6.5 | 88.9 | 0.406 | - | - |
| East wall - Styropor | 3.0 | 88.9 | 0.406 | - | - |
| West wall - Styropor | 3.0 | 88.9 | 0.406 | - | - |
| Floor wall - Styropor | 1.4 | 88.9 | 0.406 | - | - |
| | Zone 6 | | | | |
| Ceiling wall - lightweight concrete | 0.8 | 101.6 | 1.098 | - | - |
| North wall - lightweight concrete | 1.5 | 101.6 | 1.098 | - | - |
| North wall - air vent Styropor | 0.6 | 88.9 | 0.406 | - | - |
| South wall - lightweight concrete | 1.7 | 101.6 | 1.098 | - | - |
| South wall - air vent Styropor | 0.3 | 88.9 | 0.406 | - | - |
| East wall - lightweight concrete | 1.6 | 101.6 | 1.098 | - | - |
| West wall - lightweight concrete | 1.6 | 101.6 | 1.098 | - | - |
| Floor wall - lightweight concrete | 0.8 | 101.6 | 1.098 | - | - |
| | **Reference House** | | | | |
| | Zone 1 | | | | |
| Ceiling wall - Styropor | 37.1 | 88.9 | 0.406 | - | - |
| North wall - Styropor | 15.7 | 88.9 | 0.406 | - | - |
| North wall - double glazings (6.3 mm air gap) | 1.3 | 18.3 | 3.058 | 0.7 | No |
| North wall - door insulation board | 1.8 | 25.4 | 1.181 | - | - |
| South wall - Styropor | 23.3 | 88.9 | 0.406 | - | - |
| South wall - double glazings (6.3 mm air gap) | 5.2 | 18.3 | 3.058 | 0.7 | Yes |
| East wall - Styropor | 16.6 | 88.9 | 0.406 | - | - |
| West wall - Styropor | 16.6 | 88.9 | 0.406 | - | - |
| Floor wall - lightweight concrete | 35.9 | 101.6 | 1.098 | - | - |

**Table 2** Boussinesq model air properties at operating temperatures

| **Boussinesq model air properties** | **Summer** | **Winter** |
|---|---|---|
| Thermal expansion coefficient $\beta$ (1/K) | 0.0033 | 0.0036 |
| Density $\rho$ (kg/m$^3$) | 1.1512 | 1.2587 |
| Specific heat *Cp* (J/kgK) | 1.007 | 1.006 |
| Thermal conductivity *K* (W/mK) | 0.0267 | 0.0248 |
| Dynamic viscosity $\mu$ (kg/ms) | 1.905x10$^{-5}$ | 1.775x10$^{-5}$ |

**Table 3** Vent airflow velocities for summer daytime extreme

| **Vent airflow velocities for summer daytime extreme** | **Underground space vent** | **Roof vent** |
|---|---|---|
| Boundary type | Inlet | Outlet |
| Section width *x* (m) | 0.800 | 1.800 |
| Section length *L* (m) | 0.400 | 0.828 |
| Hydraulic diameter $D_h$ (boundary layer length) (m) | 0.533 | 1.134 |
| Density $\rho$ (kg/m$^3$) | 1.196 | 1.154 |
| Dynamic viscosity $\mu$ (g/ms) | 0.01848 | 0.01902 |
| Max airflow rate *v* (m$^3$/s) | 0.316 | 0.305 |
| Max freestream velocity $U_\infty$ (m/s) | 0.989 | 0.205 |
| Reynolds *Re* | 34 000 | 14 000 |
| Turbulent intensity *I* | 4.3% | 4.9% |
| Target mass flow rate $\dot{m}$ (including infiltration) (kg/s) | 0.35817 | 0.35817 |

**Table 4** Opening airflow velocities for summer daytime and winter nighttime extremes

| | **Summer Daytime Extreme** | | | | **Winter Nighttime Extreme** | | | |
|---|---|---|---|---|---|---|---|---|
| **Opening airflow velocities** | **South-side semi DSF bottom opening** | **North-side semi DSF bottom opening** | **DSR North opening** | **DSR South opening** | **South-side semi DSF bottom opening** | **North-side semi DSF bottom opening** | **DSR North opening** | **DSR South opening** |
| Section width *x* (m) | 1.600 | 1.600 | 2.000 | 2.000 | 1.600 | 1.600 | 2.000 | 2.000 |
| Section length *L* (m) | 0.700 | 0.700 | 0.150 | 0.150 | 0.700 | 0.700 | 0.150 | 0.150 |
| Hydraulic diameter $D_h$ (boundary layer length) (m) | 0.974 | 0.974 | 0.279 | 0.279 | 0.974 | 0.974 | 0.279 | 0.279 |
| Density $\rho$ (kg/m$^3$) | 1.165 | 1.181 | 1.176 | 1.175 | 1.279 | 1.270 | 1.265 | 1.266 |
| Dynamic viscosity $\mu$ (g/ms) | 0.01887 | 0.01867 | 0.01874 | 0.01874 | 0.01752 | 0.01763 | 0.01768 | 0.01767 |
| Max airflow rate *v* (m$^3$/s) | 0.286 | 0.030 | 0.028 | 0.024 | 0.118 | 0.113 | 0.110 | 0.111 |
| Max freestream velocity $U_\infty$ (m/s) | 0.255 | 0.027 | 0.095 | 0.082 | 0.105 | 0.101 | 0.368 | 0.370 |

**Table 5** Zone wall distance estimation and model airflow determination for summer daytime and winter nighttime extremes

| | Summer Daytime Extreme | | | | Winter Nighttime Extreme | | | |
|---|---|---|---|---|---|---|---|---|
| **Zone y+ wall distance estimation** | **Underground space** | **DSR** | **South-side semi DSF** | **North-side semi DSF** | **Underground space** | **DSR** | **South-side semi DSF** | **North-side semi DSF** |
| Section width *x* (m) | 2.168 | 6.958 | 2.190 | 2.190 | 2.168 | 6.958 | 2.190 | 2.190 |
| Section length *L* (m) | 1.800 | 0.155 | 0.995 | 0.995 | 1.800 | 0.155 | 0.995 | 0.995 |
| Hydraulic diameter $D_h$ (boundary layer length) (m) | 1.967 | 0.304 | 1.368 | 1.368 | 1.967 | 0.304 | 1.368 | 1.368 |
| Temperature *T* (ºC) | 28.11 | 30.05 | 29.13 | 28.61 | 5.05 | 4.27 | 3.34 | 4.38 |
| Density $\rho$ (kg/m$^3$) | 1.173 | 1.166 | 1.169 | 1.171 | 1.270 | 1.274 | 1.278 | 1.274 |
| Dynamic viscosity $\mu$ (g/ms) | 0.01876 | 0.01886 | 0.01881 | 0.01879 | 0.01762 | 0.01758 | 0.01753 | 0.01758 |
| Max airflow rate *v* (m$^3$/s) | 0.026 | 0.008 | 0.147 | 0.016 | 0.034 | 0.031 | 0.061 | 0.058 |
| Max freestream velocity $U_\infty$ (m/s) | 0.007 | 0.007 | 0.067 | 0.007 | 0.009 | 0.028 | 0.028 | 0.027 |
| Desired *y+* | 1 | 1 | 1 | 1 | 1 | 1 | 1 | 1 |
| Reynolds *Re* | 860 | 130 | 5,700 | 600 | 1,300 | 620 | 2,800 | 2,700 |
| Estimated wall distance (m) | 0.022 | 0.014 | 0.003 | 0.020 | 0.016 | 0.004 | 0.006 | 0.006 |
| **Zone airflow model determination** | **Underground space** | **DSR** | **South-side semi DSF** | **North-side semi DSF** | **Underground space** | **DSR** | **South-side semi DSF** | **North-side semi DSF** |
| Length *L* (m) | 1.800 | 0.155 | 4.281 | 2.551 | 1.800 | 0.155 | 4.281 | 2.551 |
| Specific heat *Cp* (kJ/kgK) | 1.006 | 1.006 | 1.006 | 1.006 | 1.006 | 1.006 | 1.006 | 1.006 |
| Thermal conductivity *K* (W/mK) | 0.0263 | 0.0264 | 0.0263 | 0.0263 | 0.0247 | 0.0246 | 0.0245 | 0.0246 |
| Thermal expansion coefficient $\beta$ (1/K) | 0.0033 | 0.0033 | 0.0033 | 0.0033 | 0.0036 | 0.0036 | 0.0036 | 0.0036 |
| Max temperature difference $\Delta T$ (ºC) | 5.80 | 2.61 | 1.58 | 2.52 | 1.95 | 1.92 | 2.71 | 1.81 |
| Rayleigh *Ra* | $3.1x10^9$ | $0.9x10^6$ | $11x10^9$ | $3.8x10^9$ | $1.5x10^9$ | $1.0x10^6$ | $29x10^9$ | $4.0x10^9$ |
| Airflow model | Turbulent | Transitional | Turbulent | Turbulent | Turbulent | Transitional | Turbulent | Turbulent |

**Table 6** New house and reference house under PH criteria

| **PH criteria** | **New House** | **Reference House** | **PH Criteria Limits** |
|---|---|---|---|
| Space heating demand kWh/(m$^2$yr) | 13.3 | 16.5 | <15 |
| Primary energy use kWh/(m$^2$yr) | 0 | 0 | <120 |
| Air change per hour (at max pressure of 50 Pa) | 0.195 | 0.195 | <0.6 |
| Time set-point not met during cooling | 0% | 0% | <10% |

**Table 7** Monthly energy demand and living quarters temperatures of New House and Reference House versus outside

| **Month** | **Average temperature outside (ºC)** | **Average temperature New House living quarters (ºC)** | **Average temperature Reference House living quarters (ºC)** | **Heating demand New House (kWh)** | **Heating demand Reference House (kWh)** | **Cooling demand New House (kWh)** | **Cooling demand Reference House (kWh)** |
|---|---|---|---|---|---|---|---|
| January | 5.8 | 18.3 | 17.9 | 122.7 | 151.9 | 9.9 | 2.1 |
| February | 4.9 | 17.8 | 17.7 | 192.0 | 220.4 | 2.8 | 1.6 |
| March | 7.3 | 18.0 | 18.2 | 101.8 | 113.6 | 2.5 | 2.6 |
| April | 12.2 | 20.5 | 21.3 | 6.1 | 4.1 | 3.9 | 6.1 |
| May | 16.8 | 23.1 | 24.2 | 0.1 | 0 | 26.8 | 67.7 |

| | | | | | | | |
|---|---|---|---|---|---|---|---|
| June | 21.6 | 25.4 | 25.9 | 0 | 0 | 168.7 | 252.9 |
| July | 24.1 | 26.0 | 26.3 | 0 | 0 | 293.6 | 383.6 |
| August | 24.2 | 26.2 | 26.4 | 0 | 0 | 337.0 | 416.2 |
| September | 20.8 | 25.5 | 25.9 | 0 | 0 | 191.7 | 242,4 |
| October | 16.5 | 24.9 | 24.9 | 0 | 0 | 145.0 | 112.7 |
| November | 11.4 | 21.8 | 21.0 | 3.0 | 9.3 | 37.9 | 17.3 |
| December | 7.9 | 18.2 | 17.7 | 52.4 | 91.7 | 3.3 | 1.7 |

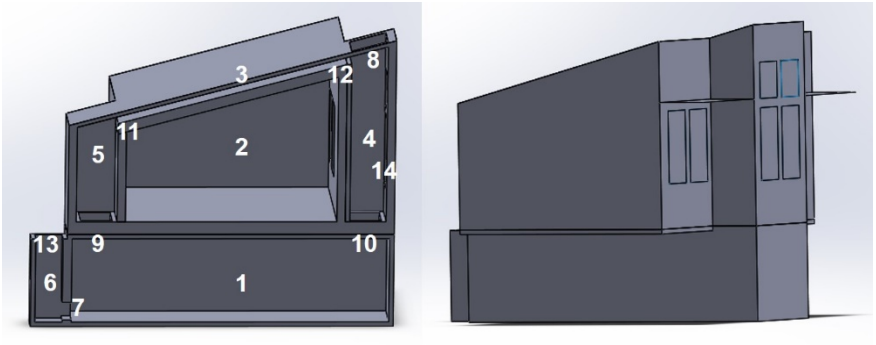


**Figure 1** New passive house

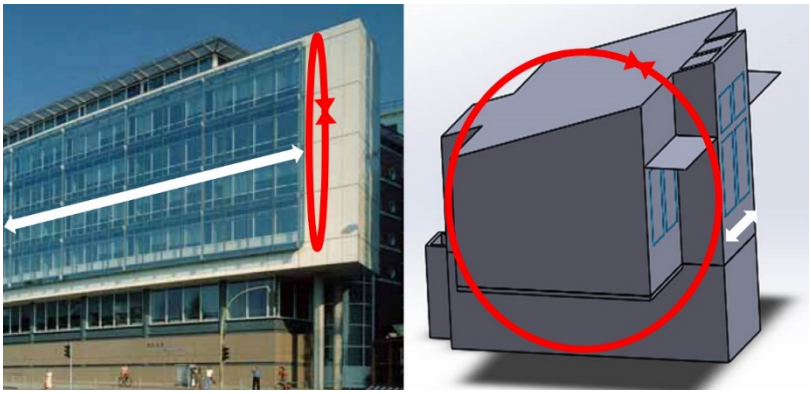

**Figure 2** Deutscher Ring Verwaltungsgebäude with full south-side DSF and no integration (Poirazis 2004) vs. new house with partial south-side and west-side DSF and full integration

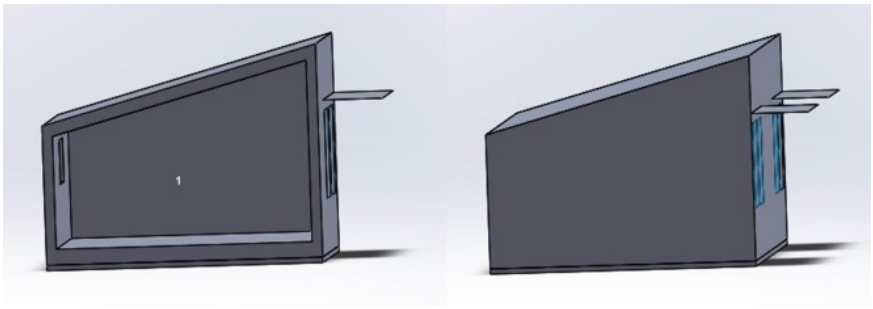

**Figure 3** Conventional reference house

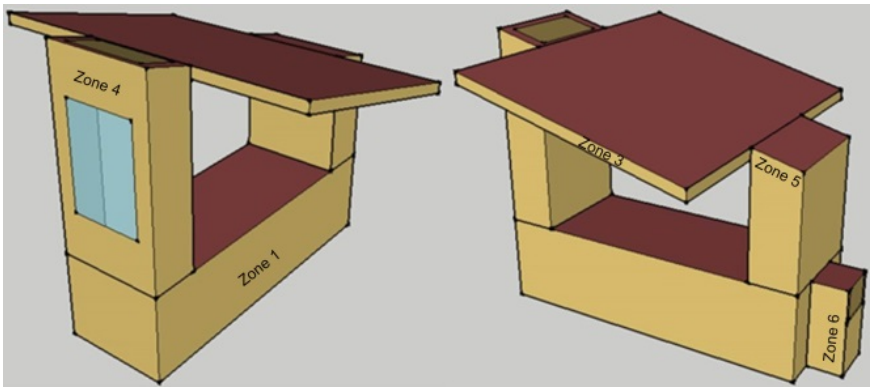


**Figure 4** DSE cavity of new house with zones

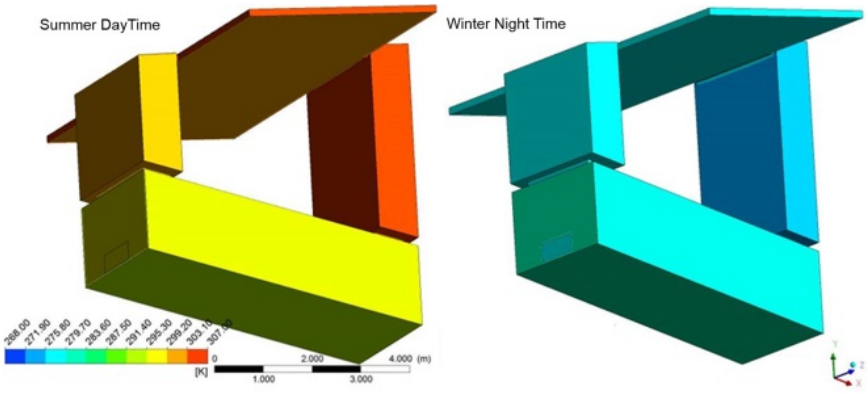


**Figure 5** Boundary conditions of new house for summer day time and winter night time extremes

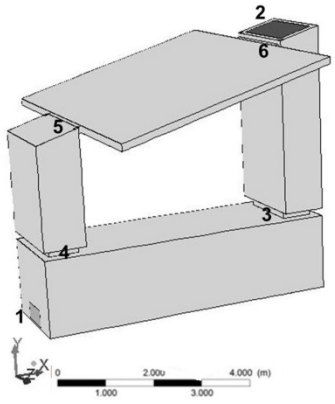


**Figure 6** Fluid domain geometry

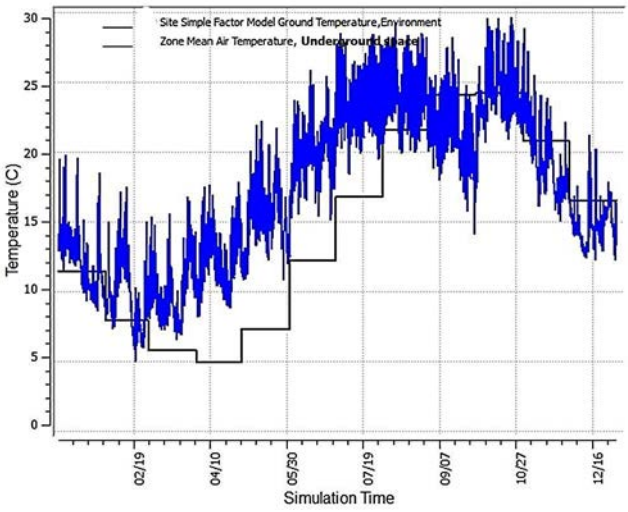


**Figure 7** Annual air temperatures in underground space versus ground

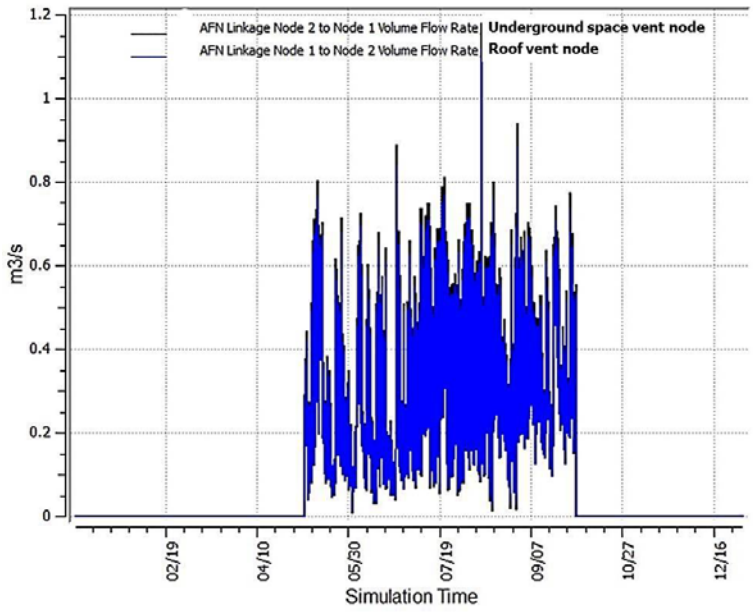


**Figure 8** Annual airflow rates at roof and underground space vent nodes

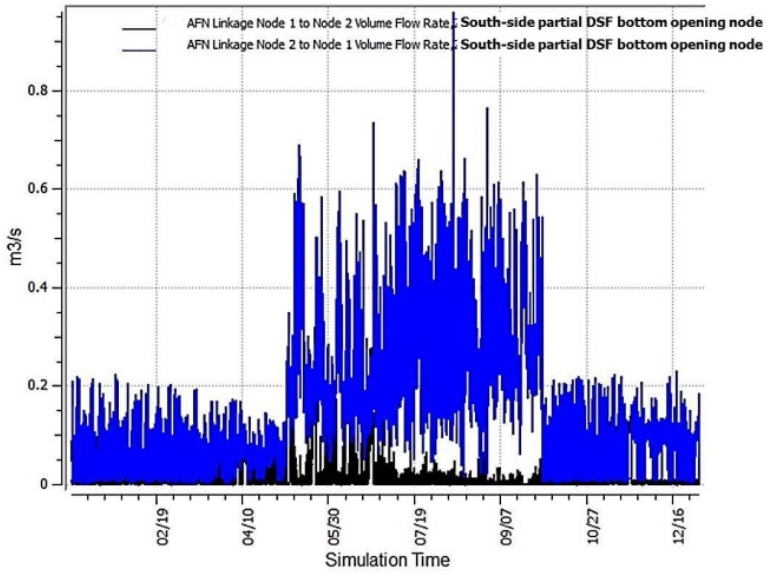


**Figure 9** Annual airflow rates at south-side partial DSF bottom opening node

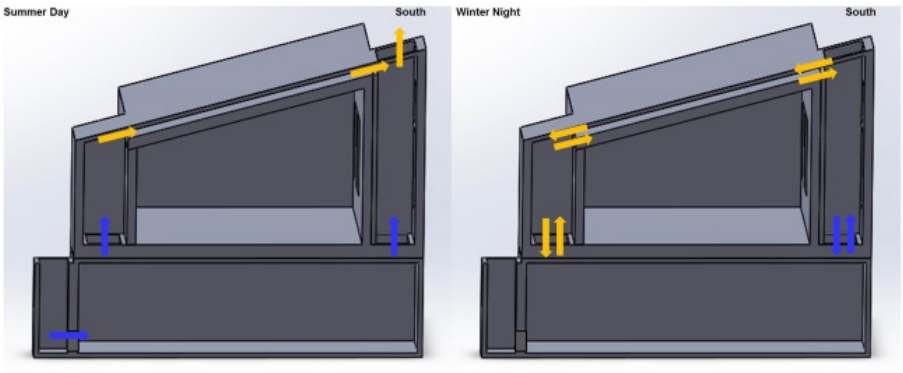


**Figure 10** Airflow paths at new house nodes on summer days and winter nights

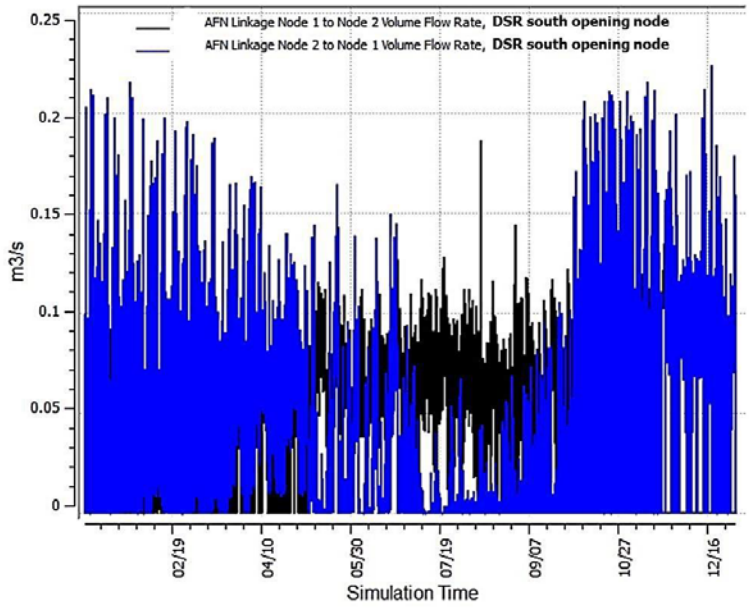


**Figure 11** Annual airflow rates at DSR south opening node

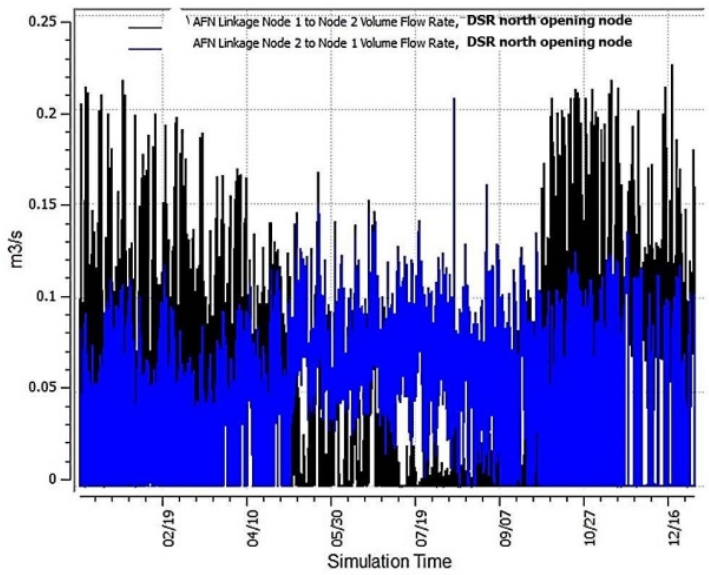


**Figure 12** Annual airflow rates at DSR north opening node

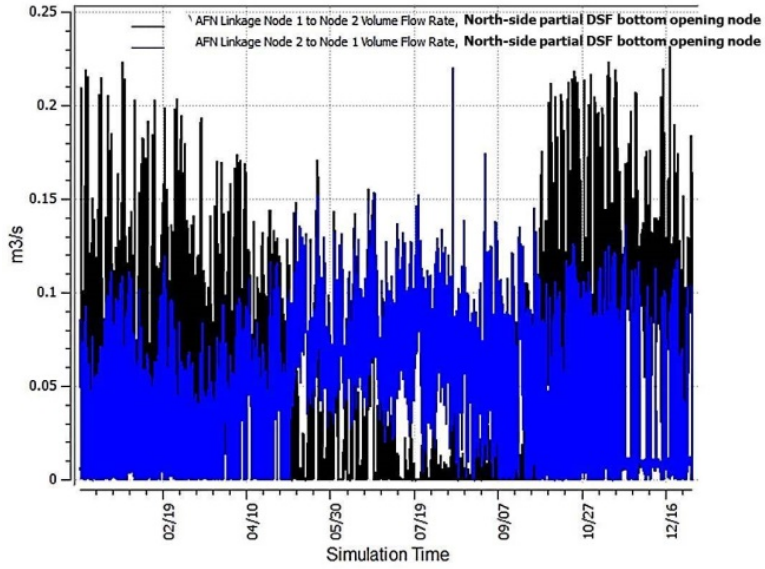


**Figure 13** Annual airflow rates at north-side partial DSF bottom opening node

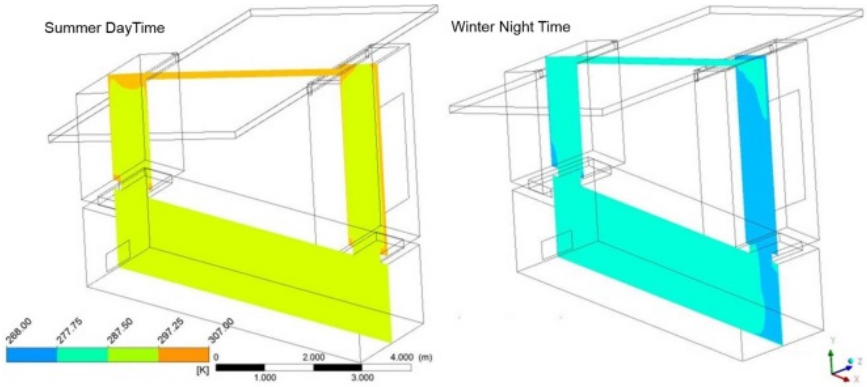


**Figure 14** Static air temperatures at mid-section of new house

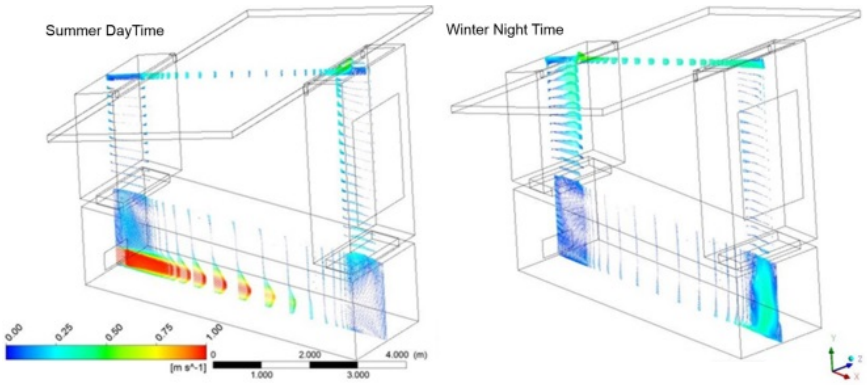


**Figure 15** Vectors of velocity magnitude at midsection of new house

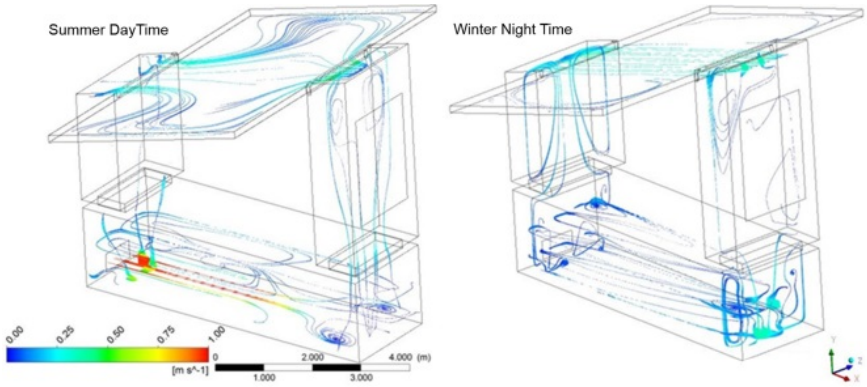


**Figure 16** Vectors of velocity magnitude at midsection of underground space, inlet, DSR and

partial DSF

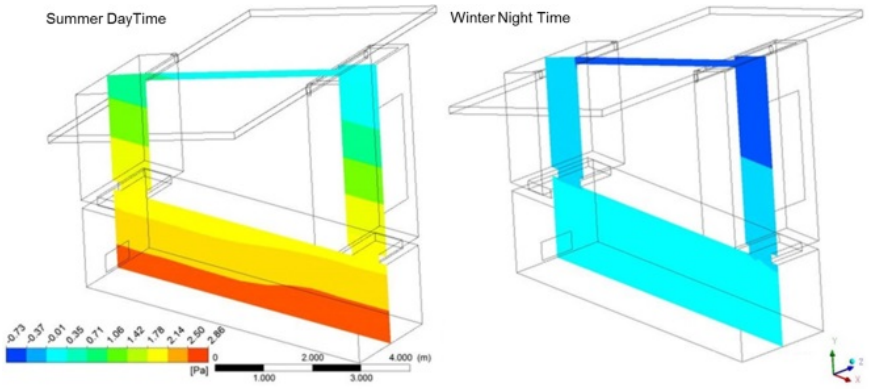


**Figure 17** Static air pressures at midsection of new house

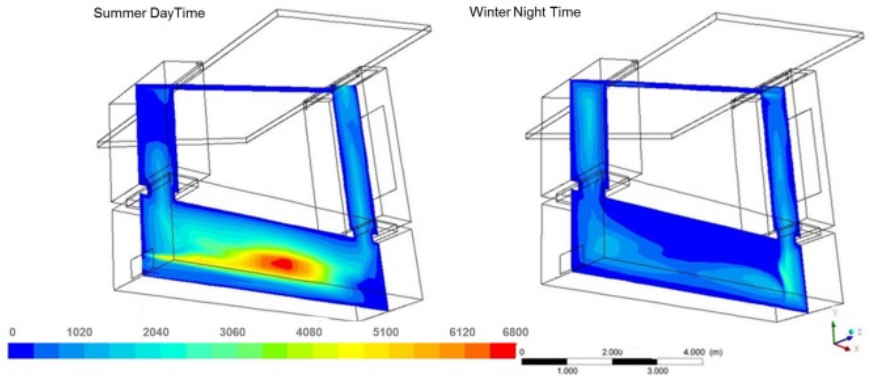


**Figure 18** Turbulent Reynolds number (*Re_y*) at midsection of new house